Radiation Measurements 176 (2024) 107175

Contents lists available at ScienceDirect

Radiation Measurements

journal homepage: www.elsevier.com/locate/radmeas

Carbon ion mono-energetic and spread-out Bragg peak measurements using nanocomposite Fricke gel dosimeters with LET-independent response

Viktoria Bayer [a,b,c,*], José Vedelago [d,a,b], Stefan Dorsch [a,b,d], Cedric Beyer [d,a], Stephan Brons [e], Wibke Johnen [a,b], Philipp Biegger [f], Ulrich Weber [g], Armin Runz [a,b], Christian P. Karger [a,b]

[a] Department of Medical Physics in Radiation Oncology, German Cancer Research Center (DKFZ), Heidelberg, Germany
[b] Heidelberg Institute for Radiation Oncology (HIRO), National Center for Radiation Research in Oncology (NCRO), Heidelberg, Germany
[c] Department for Physics and Astronomy, Heidelberg University, Heidelberg, Germany
[d] Department of Radiation Oncology, Heidelberg University Hospital (UKHD), Heidelberg, Germany
[e] Heidelberg Ion Beam Therapy Center (HIT), Heidelberg University Hospital, Heidelberg, Germany
[f] Division of Medical Physics in Radiology, German Cancer Research Center (DKFZ), Heidelberg, Germany
[g] GSI Helmholtzzentrum für Schwerionenforschung, Darmstadt, Germany

ARTICLE INFO

Keywords:
Fricke gel dosimeter
Linear energy transfer (LET)
Gel dosimetry
Carbon ion beam therapy
Nanocomposite Fricke gel (NC-FG)

ABSTRACT

This study investigates the LET-dependence of dose measurements performed with a nanocomposite Fricke gel (NC-FG) upon irradiation with carbon ion beams to address the problem of quenching of gel dosimeters in high-LET particle therapy. The preparation of the NC-FG in a simple gel preparation device was performed for atmospheric and anoxic environmental conditions and two different container materials. Irradiation was performed with carbon ion beams at energies of 133.39 MeV/u or 194.87 MeV/u, complemented by a modulated 10 mm carbon ion spread-out Bragg peak (SOBP) irradiation. The R1 profiles obtained from the MRI readout were compared to the treatment planning system and a 2D-ionisation chamber array measurement performed for the mono-energetic and SOBP irradiations, respectively. For different dose levels, no difference in the gel response was obtained for the 3D-printed plastic containers, while the glass vials exhibited a linear dose response. Additional use of the glove box changes produced similar results. For both the mono-energetic and the SOBP irradiation, a linear dose response without quenching was observed. For depths ranging up to the Bragg peak position, the mono-energetic profiles deviated by less than ±15% from the planned dose distribution, excluding the lowest entrance surface dose (ESD). For the SOBP profiles, the deviation from the measured dose distribution was less than ±10% for depths between 20 mm and 33 mm. This study presents a LET-independent measurement of mono-energetic carbon ion Bragg peaks and, for the first time, a LET-independent measurement of a carbon ion SOBP with the NC-FG prepared in a simple gel preparation device under atmospheric conditions. The NC-FG provides a possible solution for 3D dosimetry in carbon ion radiotherapy.

1. Introduction

Ion beam therapy offers the advantage of delivering a high dose to tumour tissue while sparing surrounding organs at risk. For this, mono-energetic beams of different energies are superimposed resulting in spread-out Bragg peaks (SOBP). As a special feature of ion beams, their linear energy transfer (LET) increases with increasing depth and reaches its maximum value shortly behind the Bragg peak. The increase of LET is more pronounced for heavier ions like carbon ions than for protons (Jäkel, 2020). The increased LET, however, also poses a problem for solid-state detectors used for dose measurements, resulting in a reduced detector response with increasing LET (Al-Nowais et al., 2009; Høye et al., 2017). The reduced detector response is known as "quenching" and as a result, the height of the Bragg peak is reduced relative to the dose level in the entrance channel.

While ion chambers exhibit a LET-independent response and can therefore be used for reference dosimetry (IAEA, 2000; Vedelago et al., 2022), their spatial resolution is rather low and limited to 2D measurements when arranged in an array. In contrast, gel dosimeters can

* Corresponding author at: Department of Medical Physics in Radiation Oncology, German Cancer Research Center (DKFZ), Heidelberg, Germany.
E-mail address: viktoria.bayer@dkfz.de (V. Bayer).

https://doi.org/10.1016/j.radmeas.2024.107175
Received 14 December 2023; Received in revised form 30 April 2024; Accepted 20 May 2024
Available online 28 May 2024

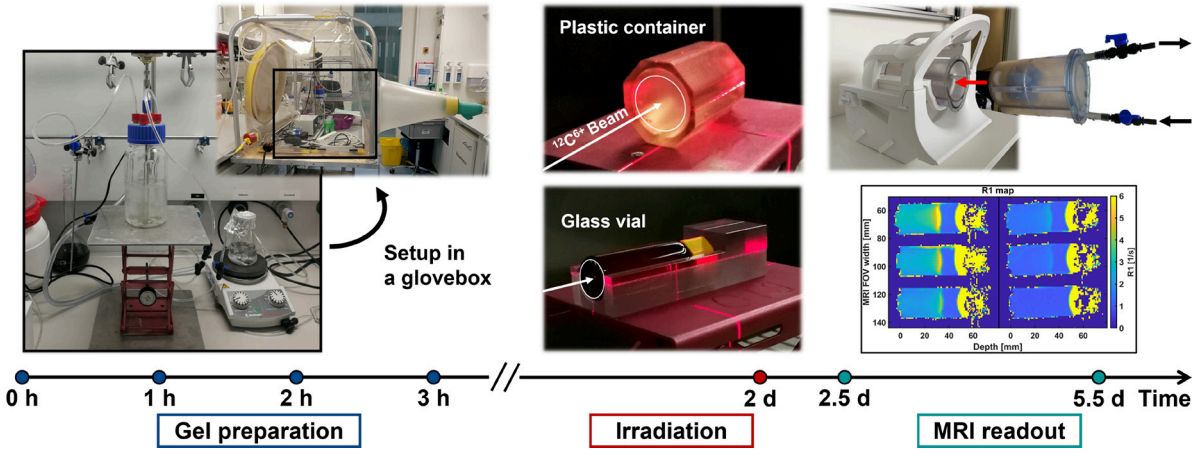

Fig. 1. Workflow of the experiments. The gel preparation setup was positioned in a fume hood, except for a single batch where it was placed in a glove box containing a nitrogen atmosphere. The positioning for irradiation and MRI readout in a water-flow phantom is shown for the plastic and glass container experiments.

achieve true 3D dose distributions based on chemical processes in the gel induced by the ionising radiation (De Deene, 2022; Macchione et al., 2022), however, the response of gel dosimeters is in general LET-dependent (Stiefel et al., 2004; Gustavsson et al., 2004; Hillbrand et al., 2019; Vedelago et al., 2021). While a few gel dosimeters have been shown to be LET-independent for proton beams (Zeidan et al., 2010; Yao et al., 2023), most gel dosimeters show a significant quenching effect for carbon ion beams (Ramm et al., 2000; Kantemiris et al., 2009; Maeyama et al., 2015; Hayashi et al., 2021). The quenching effect arises from a high concentration of radiolysis products in water leading to an increased recombination of radicals to molecules within the Bragg peak region. To address this issue, Maeyama et al. (2014) proposed a nanocomposite Fricke gel (NC-FG). The addition of nanoclay, constructing the gel matrix of the Fricke gel, results in a LET-independent response of the gel (Maeyama et al., 2016).

A further interesting aspect of gel dosimeters is that they may also be used in anthropomorphic phantoms as has been shown recently for polymer gels, that undergo polymerisation after irradiation (Elter et al., 2021b), or Fricke gels, which utilise oxidation of embedded ferrous ions (Rousseau et al., 2023) in conventional photon therapy. However, for gel dosimeters, the container material has to be carefully selected (Elter et al., 2019). It has been reported that some gel dosimeters are sensitive to oxygen contamination, which has to be considered by sealing the container with suitable materials and by using oxygen scavengers in the gel composition (Fong et al., 2001; Jaszczak et al., 2019), or by preparing the gel in a glove box (Mizukami et al., 2021).

In this study, NC-FG dosimeters are used to measure mono-energetic and spread-out carbon ion Bragg peaks. The LET independence is analysed quantitatively for different initial energies and within an SOBP. In addition, the effect of the container material on the gel response was quantified, and a simple preparation device was tested with and without the additional use of a glove box.

2. Materials and methods

2.1. Gel preparation

The gel preparation procedure is based on the publication of Mizukami et al. (2021). The nanocomposite Fricke gel (NC-FG) consists of 98% ultrapure water, 2% nanoclay (Laponite-XLG XR; BYK-Chemie GmbH, Wesel, Germany) and 1 mM ammonium iron(II) sulfate hexahydrate (ROTI®METIC, Karlsruhe, Germany). The components were mixed at room temperature under air-free conditions in a simplified version of a gel preparation device developed by Runz et al. (2023). The gel preparation setup is shown in Fig. 1 and consists of a sealed glass bottle positioned on top of a lab jack to easily adjust the height. The bottle is connected to a vacuum pump and a nitrogen source via plastic tubes to maintain a constant nitrogen gas flow. A metal rod with a rotating blade was used with an adjustable motor to ensure uniform mixing. The components were added via a funnel in the hole of the glass bottle lid. To test the potential advantage of a gel preparation environment under completely anoxic conditions, the whole setup was additionally used inside a glove box (Basic Vinyl Glove Box; Coy Laboratory Products Inc., Grass Lake, USA) for one batch production of the gel (Fig. 1).

For gel preparation, 480 mL and 120 mL of ultrapure water in a glass bottle and a beaker, respectively, were purged with nitrogen gas for 60 min with constant mixing. Next, 12 g nanoclay was added to the water in the glass bottle and mixed for 60 min. During the mixing process, the nitrogen gas was flushed above the solution. Then, 236 mg of ammonium iron(II) sulfate hexahydrate was dissolved in the beaker with a magnetic stirrer. This solution was added to the glass bottle with the 480 mL of water and mixed for another 60 min. The NC-FG was filled via a tube with a positive nitrogen pressure either into cylindrical, 3D-printed screw-lid containers (VeroClear; Stratasys, Israel) with a volume of 58 mL and 115 mL (35 mm diameter, 60 mm and 120 mm height) or into screw-lid amber glass vials of 20 mL volume (20 mm diameter, 60 mm height). To minimise gas bubbles, the glass vials were centrifuged in a rotation mixer (Laboratory centrifuge CD-0412-50; Phoenix Instrument GmbH, Garbsen, Germany) at 1600 rpm for 3 min. The gel containers were flushed with argon gas before the filling. The containers were stored in the lab (under atmospheric conditions) to solidify for 2 days before irradiation.

2.2. Irradiation

The irradiation was performed at the Heidelberg Ion-Beam Therapy Center (HIT) using a scanned 20 mm diameter circular shaped $^{12}C^{6+}$ beam at energies of 133.39 MeV/u or 194.87 MeV/u, corresponding to water-equivalent ranges of 37.31 mm and 77.33 mm. The field was generated by beam scanning using pencil beams of 7 mm FWHM focus width and a lateral step size of 1 mm. A 3 mm ripple filter was used (Weber and Kraft, 1999), and entrance surface doses (ESD) from 87 Gy up to 766 Gy were applied. In addition, a 10 mm spread-out Bragg peak (SOBP) was generated passively using a range modulator (Simeonov et al., 2021) together with the 133.39 MeV/u beam. The range modulator was positioned upstream at a distance of 80 cm from the entrance surface of the container.

The centre of the gel containers was positioned at the isocenter, as shown in Fig. 1, for irradiation through the container bottom. The glass vials were placed within a 3D-printed holder (VeroClear; Stratasys, Israel). For the higher energy, a 40 mm water-equivalent bolus was

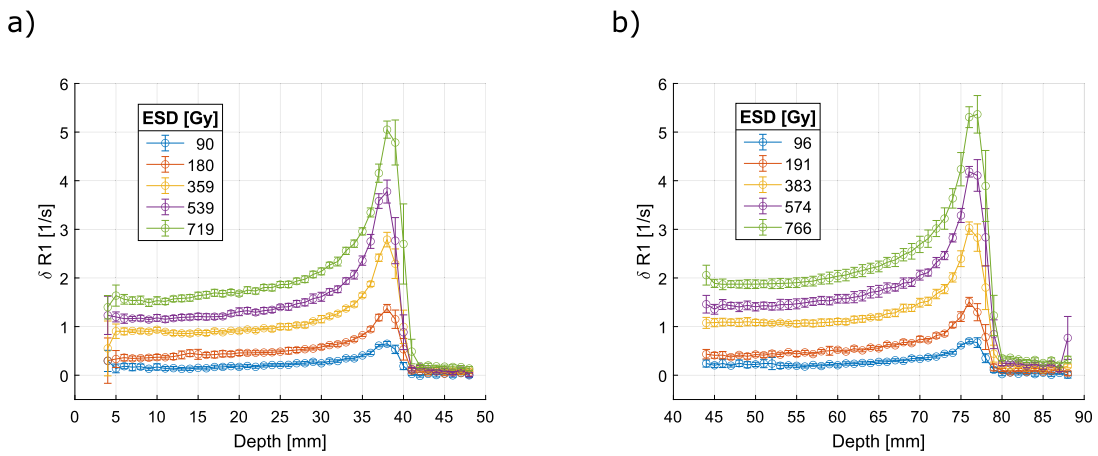

Fig. 2. δR1 profiles of NC-FG filled into glass vials and irradiated with carbon ions of 133.39 MeV/u (a) or 194.87 MeV/u (b). For the higher energy, the ion range in the vials was reduced by an additional 40 mm water-equivalent bolus.

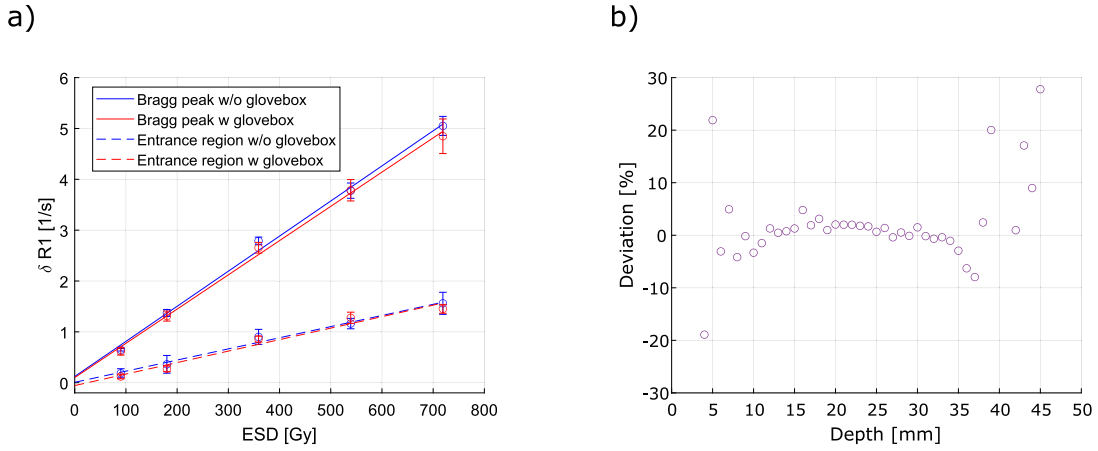

Fig. 3. Environmental influence on the gel response when irradiated with mono-energetic carbon ion beams of 133.39 MeV/u and a ESD range between 90 Gy and 719 Gy. Representative linear fits are shown for the entrance region at 6 mm and the Bragg peak at 38 mm, for the preparation done with and without a glove box (a). Deviation of the slopes for the gel prepared with and without a glove box (b).

positioned in front of the vials to adjust the range of the beam in the vials to that of the lower energy.

For the mono-energetic beams, the reference depth dose distributions and LET values were taken from the database of the treatment planning system (TPS) (RayStation® 13A; RaySearch Laboratories, Stockholm, Sweden). As the range modulator has not been implemented in the TPS, the relative depth dose distribution of the SOBP has been measured with a single detector element of a 2D ionisation chamber array (OCTAVIUS Detector 1000 SRSp; PTW, Freiburg, Germany) using PMMA plates to modulate the range. The absolute ESD values for both the mono-energetic beams and the SOBP were determined at a water-equivalent thickness of 7.03 mm using a pinpoint ion chamber (PinPoint Ion Chamber 31015; PTW, Freiburg, Germany).

2.3. MRI readout

Spatial distribution of T1 relaxation time was determined using a 1.5 T diagnostic MRI scanner (MAGNETOM Sola; Siemens Healthineers, Erlangen, Germany) with a head/neck coil (BioMatrix Head/Neck 20, Siemens Healthineers, Erlangen, Germany) 14 h and 3 days after irradiation. The readout was performed with a saturation recovery sequence with a flip angle of 25°, an echo time (TE) of 3.82 ms, 35 different inversion times (TI) ranging from 20 ms to 4000 ms and repetition times (TR) from 45 ms to 4030 ms. A 5 mm thick slice was reconstructed in the coronal plane, positioned at the centre of the gel containers with a pixel size of (1×1) mm^2. The field-of-view (FOV) was (160×160) mm^2 for the plastic containers and (192×192) mm^2 for the glass vials. All irradiated containers plus one non-irradiated container were positioned in an in-house developed water-flow phantom, shown in Fig. 1, as described in Elter et al. (2021a). The phantom is filled with water mixed with 4 mmol/L contrast agent (GADOVIST®; Bayer AG, Leverkusen, Germany) and connected via plastic tubes to a circulation pump (refrigerated circulator F6/C25; Thermo Haake GmbH, Karlsruhe, Germany) pumping the liquid with a laminar flow at a constant temperature of (22.0±0.1) °C. To achieve accurate positioning of both the phantom and the glass containers within, 3D printed insets were employed (Fig. 1).

2.4. Post-processing

The R1 (= 1/T1) maps were computed each with 35 images by a pixel-wise exponential fit (Fig. 1). From these maps, R1 profiles were determined by averaging over a region of interest of (10×5) mm^2 at each depth. The baseline corrected δR1 profiles were then calculated by subtracting these values from the average R1 value measured in a non-irradiated container. The profiles were shifted to the same Bragg peak position and the first 4 mm including the container bottom were not evaluated due to image artefacts.

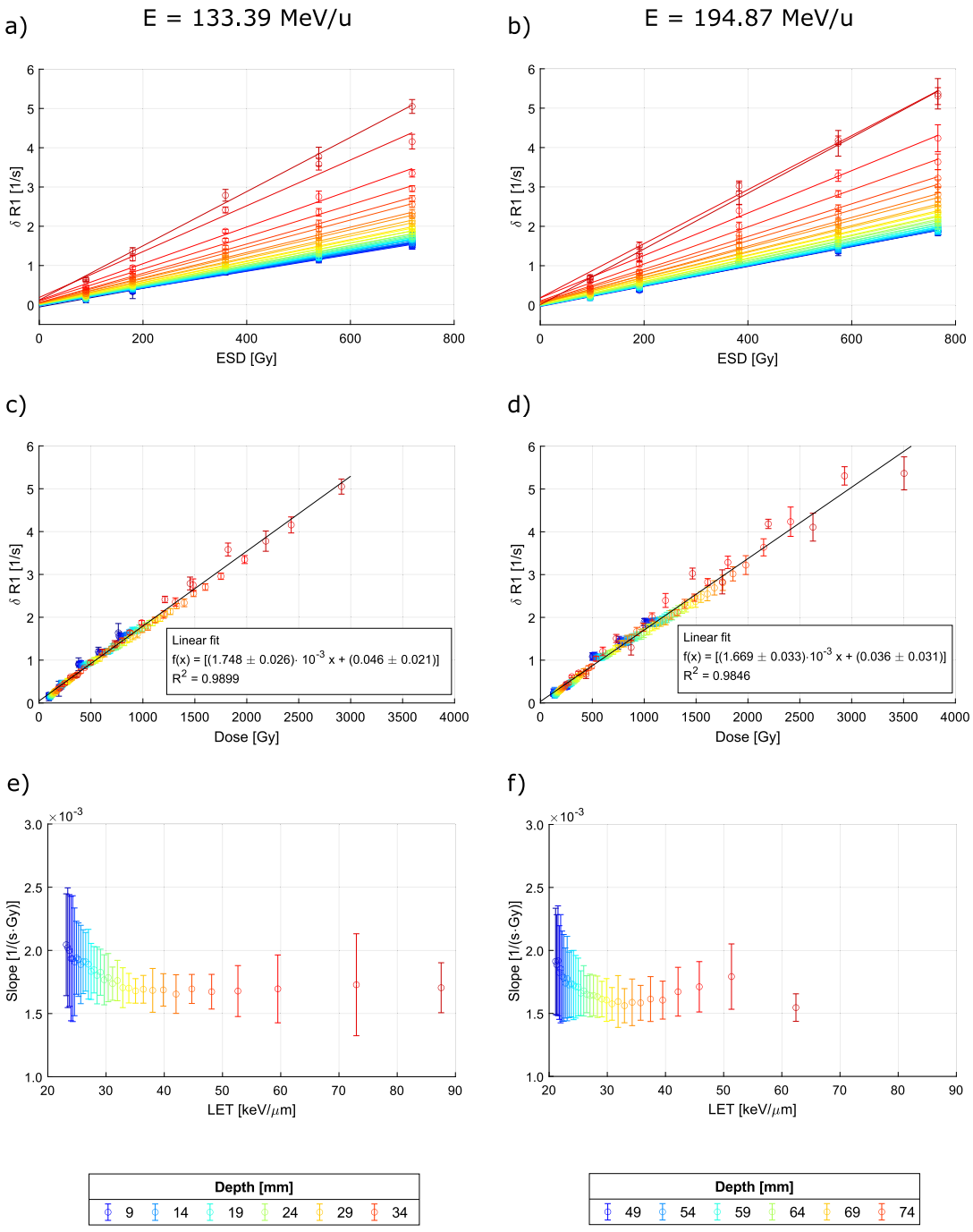

Fig. 4. Dependence of the gel response on ESD (a, b) and local dose (c, d) for both energies. The dependence of the gel sensitivity, described by the slope of the linear curves in (a, b), as a function of the corresponding LET (e, f) reveals no significant LET dependence for both energies.

3. Results

3.1. Container material

The influence of the two container materials on the gel response was analysed by the δR1 profiles for the two mono-energetic beams. For the plastic containers, the δR1 profiles for different ESD could not be separated in the entrance region (Supplementary Fig. S1). In contrast, the δR1 values for the glass vials increase proportionally with increasing ESD as shown in (Fig. 2). Consequently, all further experiments were performed with the glass vials.

3.2. Environmental influence

To assess the influence of the environmental conditions during gel preparation on the gel sensitivity, the gel was prepared with and without a glove box. Linear fits of the δR1 values against ESD obtained for both methods are shown in Fig. 3 (a) for two representative depths. For all depths from 5 mm up to the Bragg peak position at 38 mm, an $R^2 > 0.98$ was obtained from the fit. Beyond the Bragg peak, linear fits are not feasible due to the low and noisy signal in this region. The deviation between the slopes for the gel response with and without the glove box as a function of depth is shown in Fig. 3 (b). The

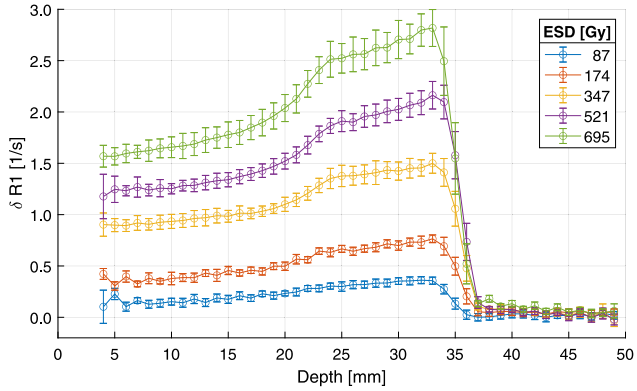

Fig. 5. δR1 profiles of NC-FG irradiated with a 10 mm carbon ion SOBP using different ESD.

deviation is below ± 5% except for the entrance region and close to the Bragg peak, where larger uncertainties are likely because of effects of the glass bottom and the limited MRI resolution in regions of steep gradients, respectively. The slopes show no significant differences for gel preparation with and without the glove box. Therefore all further experiments were performed without using the glove box.

3.3. LET-dependence of the gel sensitivity

The dependence of the gel response on ESD for the two mono-energetic carbon ion beams is shown in Figs. 4 (a) and (b). Linear fits at depths from 5 mm up to the Bragg peak position at 45 mm revealed an $R^2 > 0.98$, supporting a linear dose dependence. Using the depth dose curve from the TPS, ESD was converted into local dose. As a result, the dependence of δR1 on local dose turned out to be well described by linear fits (Fig. 4 (c) and (d), $R^2 > 0.98$) for both beam energies. The parameters of the linear regressions are given in the figures' inserts and the number of significant digits was displayed according to the GUM (2008) guidelines. Figs. 4 (e) and (f) display the sensitivity of the gel for both carbon ion beam energies as described by the slopes of linear fits as a function of the corresponding LET.

For the SOBP, the δR1 profiles obtained for the increasing ESD levels are depicted in Fig. 5. In Fig. 6 (a) the δR1 values for all depths as a function of ESD are displayed. For each depth between 5 mm up to 33 mm, a linear fit was performed ($R^2 > 0.98$ for all depths). After converting ESD into local doses by means of the measured and interpolated SOBP dose profile, the dependence of the gel response on local dose is well described by a linear relation (Fig. 6 (b)). Fitting a single linear function reveals $R^2 > 0.82$.

3.4. Comparison to the reference dose distribution

For the comparison with the reference dose distribution from the TPS, all mono-energetic profiles were normalised to one at the Bragg peak position (Figs. 7 (a) and (b)) for each beam energy. In addition, the profiles of the TPS were shifted to match the Bragg peak positions with that of the gel profiles. Figs. 7 (c) and (d) display the deviations between TPS and the gel response as a function of depth. For depths ranging up to the Bragg peak position, the deviation remains below ±15% for both energies, excluding the lowest ESD. Only at shallower depths, the deviations increase and reach values of up to ±30%.

For the comparison of the SOBP measurement with the reference data measured with the Octavius detector, all profiles were normalised to one at the mid-SOBP position at a depth of 29 mm (Fig. 8 (a)). Deviations between the NC-FG profiles and the reference profile are shown in Fig. 8 (b). Between 5 mm and 35 mm, all deviations are below ±21%, and only the lowest ESD level shows significantly larger deviations. Notably, the deviations are below ±10% for all ESD values for depths between 20 mm and 33 mm.

4. Discussion

In ion beam radiotherapy, e.g. with carbon ions, the quenching effect in the Bragg peak region remains still a problem for most gel dosimeters (Ramm et al., 2000; Kantemiris et al., 2009; Maeyama et al., 2015; Hayashi et al., 2021). In this study, a LET-independent response of the NC-FG was obtained for carbon ion beams, which allows measuring mono-energetic beams as well as SOBPs. This was demonstrated for two different energies and a 10 mm SOBP, confirming the findings of previous studies by Maeyama et al. (2014, 2017), and later followed up by Mizukami et al. (2021). Using nanoclay for the gel matrix in the Fricke gel made it possible to perform LET-independent measurements of carbon ion beams either with MRI in the case of NC-FG (Maeyama et al., 2014, 2016, 2017; Mizukami et al., 2021) or more recently with an optical readout for nanoclay radio-fluorogenic gel (Maeyama et al., 2023, 2024).

4.1. Gel production and handling

Radiosensitivity changes or even inactivation of dosimetry gels by contamination from the container material or by oxygen is well known (De Deene, 2022) and poses limitations on the selection of container materials and the gel preparation conditions. The container material can have a direct influence on the NC-FG response. For 3D-printed plastic containers, no distinguishable signals were detected in the entrance region, despite applying distinctively different doses (Supplementary Fig. S1). In contrast, this was possible with the glass vials, where the δR1 values increased linearly with increasing ESD (Fig. 2). While the same 3D-printing material has previously been successfully used for polymer gels (Elter et al., 2019), this was not possible for NC-FGs and previous studies with NC-FG were always performed with glass vials (Maeyama et al., 2014, 2016, 2017; Mizukami et al., 2021). This may reveal a problem for the construction of anthropomorphic phantoms with inserted gel dosimeters (Elter et al., 2021b; Rousseau et al., 2023) as the wall of the glass vials is visible in CT- and MR-images. Potential reasons for the inconsistent results in the 3D-printed containers may be the diffusion of atmospheric oxygen through the walls or oxygen bound in the material (Chacón et al., 2019), or contaminations of the gel by other molecules from the container material (Karger et al., 2024). Further studies with other 3D-printing materials and different storing conditions might help to overcome this issue (Elter et al., 2019).

In general, gel dosimeters have a complex production procedure that has to follow fixed protocols to achieve reproducible results (Elter et al., 2021a). For example, gels containing gelatin or agarose as gelling agents have to be cooled and heated at certain rates, which adds further steps to the process (Rousseau et al., 2023; Yao et al., 2023; Hayashi et al., 2021). NC-FG has a simpler preparation procedure due to the gelatin-free nanoclay composition, however, NC-FG is also known to be inactivated by oxygen contamination. Therefore, the gel preparation was performed in a glove box in previous studies (Maeyama et al., 2014, 2016, 2017; Mizukami et al., 2021). To investigate the impact of residual atmospheric oxygen on the NC-FG sensitivity, the use of a glove box during gel preparation was now tested in combination with a dedicated device (Runz et al., 2023). The results of this test clearly showed that the glove box has no additional benefit and that the less complex setup is sufficient to produce the NC-FG (Fig. 3).

4.2. LET-dependence quantification

As demonstrated by this study and previous investigations by Maeyama et al. (2016) for mono-energetic carbon ion beams of different energies, the NC-FG shows a linear dependence of $\delta R1$ on ESD from the entrance region to the Bragg peak. Maeyama et al. (2017) reported a slope of $1.8 \cdot 10^{-3}\,\mathrm{s^{-1}Gy^{-1}}$ in the entrance region, in agreement with the values reported in Fig. 4. As one step further,

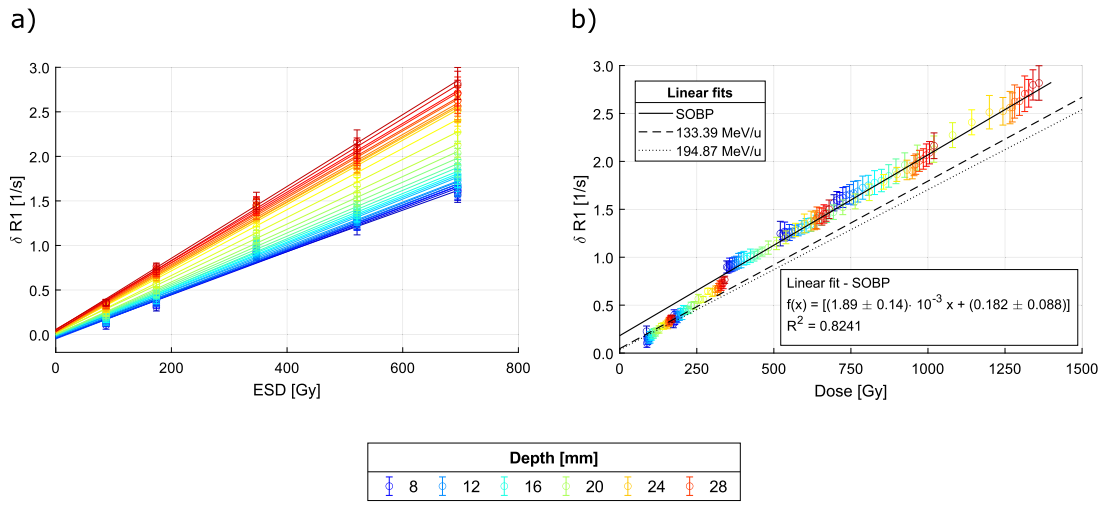

Fig. 6. Dependence of the gel response on ESD (a) and local dose (b) for a 10 mm carbon ion SOBP together with linear fits. For comparison, the linear fits for the mono-energetic beams (b) are also shown as dashed and dotted lines.

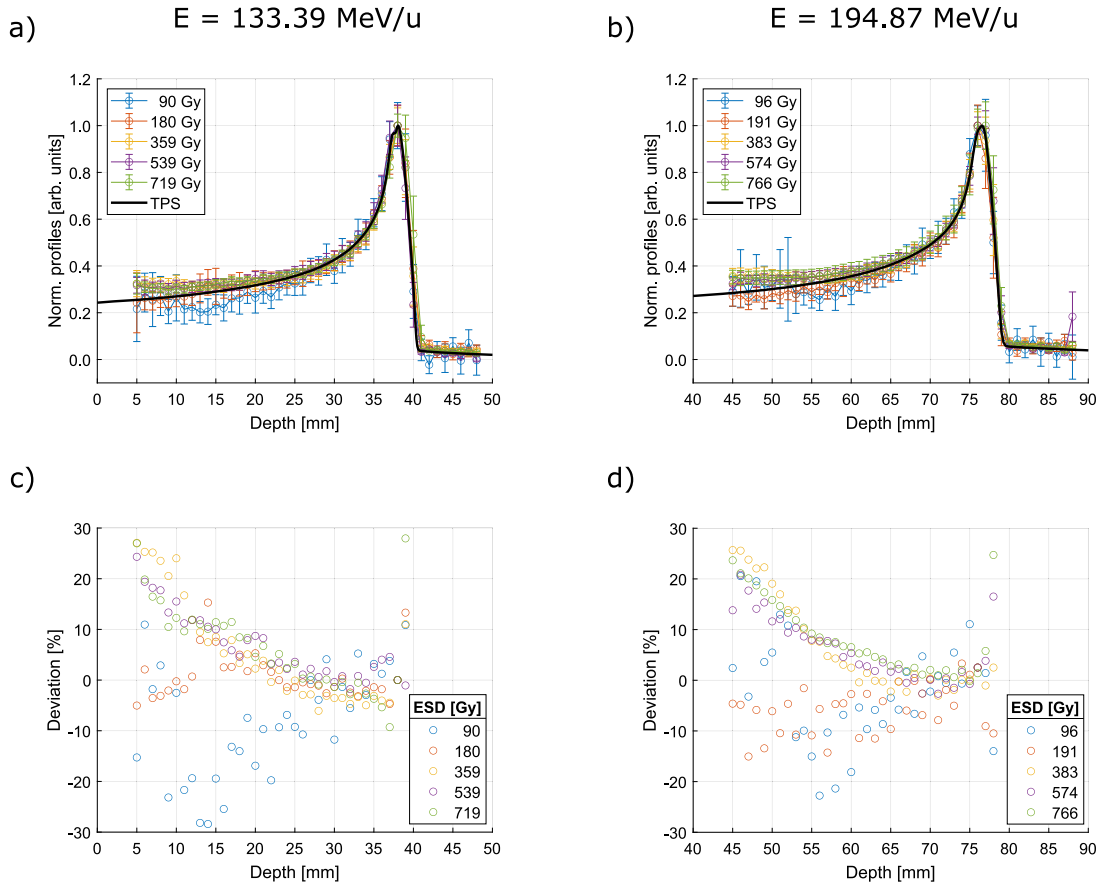

Fig. 7. Profiles measured in the NC-FG compared with the reference depth-dose curve from the TPS for the two mono-energetic carbon ion beams (a, b). Profiles were shifted to match the Bragg peak positions and were normalised to the peak dose. Deviations between each NC-FG profile and the dose values from the TPS (c, d) for both beam energies.

Figs. 4 (c) and (d) report the $\delta R1$ dependence on local dose, which can be described by a single fit, independently of the selected depth and hence LET. This finding indicates a LET-independent response of the NC-FG for both investigated energies (Figs. 4 (e) and (f)).

Ions being delivered by different initial beam energies but having the same residual range and thus residual energy differ mainly by the lower LET for the higher initial beam energy, due to the increased range straggling. In principle, this could affect the gel response, however, considering the demonstrated LET-independence of the NC-FG, the same response may be expected, which would result in the same slope of the linear fits for both energies. The remaining small difference between the slopes of the fits for the two energies may originate from additional uncontrolled factors in the production and evaluation of the gel, such as the temperature history. Overall, a direct comparison of the gel sensitivity as a function of LET showed that the NC-FG response is essentially independent of LET within experimental uncertainties.

The findings for the two mono-energetic beams have been further confirmed for the 10 mm SOBP. It has to be noted, that the increase of

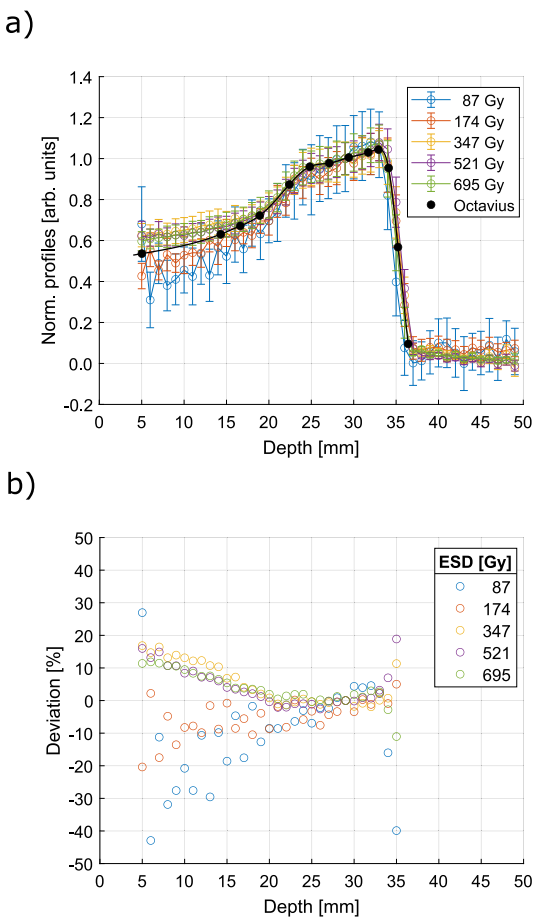

Fig. 8. Comparison of SOBP gel response and reference dose profiles (a). Deviations between gel responses and reference dose profiles are shown in (b). The measured dose profile was interpolated by splines and all profiles were normalised to one at the mid-SOBP position.

the SOBP towards the distal edge arises from the modulator, which has been optimised for a larger field size (for details, see Supplementary Fig. S2). Again a linear dose dependence on ESD was found for all depths and hence LET-values and after transforming ESD into local dose using the measured and interpolated SOBP dose profiles, the data could be described by a single linear fit. This could be expected as the difference in the initial energies is much smaller than in the experiments with the two mono-energetic beams where nearly the same slopes were found. Nevertheless, two striking effects were visible in the $\delta R1$ dependence on local dose for the SOBP: (i) while the slope of the linear fit was well comparable with those of the mono-energetic experiments, the fit curve for the SOBP was shifted to slightly higher $\delta R1$ values by an offset; (ii) regarding the data points, there was a step in $\delta R1$ direction between the two lowest and the three higher ESD levels. These findings might be explained by uncertainties in the MRI-based NC-FG evaluation, which could also influence the baseline measurements in the non-irradiated container. During the MRI measurement, the non-irradiated container and the two containers irradiated with the lowest dose were positioned in the lower row of the water-flow phantom, while the three higher doses were positioned in the upper row. Thus, some factors related to the MRI, or even some other uncontrolled factors affecting the gel itself, may have systematically influenced the relative response of the containers.

Based on the finding that the NC-FG response is LET-independent and linearly dependent on dose, it is expected that the depth curve of the gel response strictly follows the respective depth dose distribution. This has been tested by normalising the measured gel response curves for the mono-energetic beams and the SOBP to the Bragg peak or the centre of the SOBP, respectively, and by comparing these distributions with the respective dose profiles normalised in the same way (Figs. 7 and 8). As a result, a generally good agreement of the NC-FG and dose profiles was obtained. Only below depths of 20 mm, systematic deviations were observed, which have not yet been fully understood and which have to be further investigated.

4.3. Advancements and limitations

To the best of the authors' knowledge, this is the first quantification of a carbon ion SOBP with the NC-FG (Fig. 5). In previous studies, only mono-energetic carbon ion beams were used (Maeyama et al., 2016, 2017; Mizukami et al., 2021). Furthermore, the NC-FG dose response is now reported by fitting the $\delta R1$ values to the local dose, resulting in a uniform sensitivity for all LET values and a linear dose response. Lastly, a detailed comparison to the reference dose distributions is presented. These results were obtained in a simple gel preparation procedure, without the need of using a glove box.

A current limitation of the use of NC-FG in clinical investigations is the rather low sensitivity requiring doses of several hundred Gy. The development of radio-fluorogenic NC-FG has been shown to increase the gel sensitivity, thereby reducing the doses to a clinically more feasible range of 10 Gy to 40 Gy (Maeyama et al., 2023, 2024). A disadvantage of radio-fluorogenic NC-FG gels is that an optical CT system is needed for the evaluation of 3D dose distributions. In contrast, MRI is usually available in clinical institutions and evaluation protocols are easier to establish. Therefore, further development of the NC-FG towards higher sensitivity is desirable also for MRI readout.

Regarding the MRI readout, it would also be desirable to use a more efficient sequence as the applied saturation recovery sequence has an acquisition time of approximately 45 min making it not suitable for 3D scans. Alternatively, the variable flip angle spoiled gradient recalled echo (VFA-SPGR) (Mizukami et al., 2021) or the T1 FLASH method (Wang et al., 2015; Voit et al., 2020) could be used for faster R1 acquisition after reliability and stability of the signal has been investigated.

5. Conclusion

In this study, depth dose profiles of mono-energetic carbon ion beams and, for the first time, a carbon ion SOBP were measured with a nanocomposite Fricke-gel (NC-FG). The response of the NC-FG was found to be independent of the LET and linearly dependent on dose, yielding depth profiles that matched the reference dose profiles. In addition, two container materials have been tested, resulting in better signals for glass vials in comparison to 3D-printed plastic containers. For the gel preparation, a simple air-free gel preparation device has proven to be sufficient and the additional use of a glove box has been shown to be not necessary. The NC-FG dosimeter with a LET-independent response allows three-dimensional dose measurements in carbon ion radiotherapy.

CRediT authorship contribution statement

Viktoria Bayer: Writing – review & editing, Writing – original draft, Visualization, Validation, Software, Methodology, Investigation, Formal analysis, Data curation, Conceptualization. **José Vedelago:** Writing – review & editing, Writing – original draft, Supervision, Project administration, Investigation, Conceptualization. **Stefan Dorsch:** Writing – review & editing, Investigation, Conceptualization. **Cedric Beyer:** Writing – review & editing, Investigation. **Stephan Brons:** Writing – review & editing, Resources, Investigation. **Wibke Johnen:** Writing – review & editing, Resources. **Philipp Biegger:** Writing – review & editing, Resources, Investigation. **Ulrich Weber:** Writing – review & editing, Resources. **Armin Runz:** Writing – review & editing, Resources, Investigation. **Christian P. Karger:** Writing – review & editing, Writing – original draft, Supervision, Resources, Project administration, Conceptualization.

Declaration of competing interest

The authors declare that they have no known competing financial interests or personal relationships that could have appeared to influence the work reported in this paper.

Data availability

Data will be made available on request.

Acknowledgements

The authors are grateful to Dr. Takuya Maeyama for the helpful discussions, especially those on the fabrication of the gel.

Appendix A. Supplementary data

Supplementary material related to this article can be found online at https://doi.org/10.1016/j.radmeas.2024.107175.

References

Al-Nowais, S., Doran, S., Kacperek, A., Krstajic, N., Adamovics, J., Bradley, D., 2009. A preliminary analysis of LET effects in the dosimetry of proton beams using PRESAGE™ and optical CT. Appl. Radiat. Isot. 67, 415–418. http://dx.doi.org/10.1016/j.apradiso.2008.06.032.

Chacón, D., Vedelago, J., Strumia, M.C., Valente, M., Mattea, F., 2019. Raman spectroscopy as a tool to evaluate oxygen effects on the response of polymer gel dosimetry. Appl. Radiat. Isot. 150, 43–52. http://dx.doi.org/10.1016/j.apradiso.2019.05.006.

De Deene, Y., 2022. Radiation dosimetry by use of radiosensitive hydrogels and polymers: Mechanisms, state-of-the-art and perspective from 3D to 4D. Gels 8, 599. http://dx.doi.org/10.3390/gels8090599.

Elter, A., Dorsch, S., Mann, P., Runz, A., Johnen, W., Karger, C.P., 2019. Compatibility of 3D printing materials and printing techniques with PAGAT gel dosimetry. Phys. Med. Biol. 64, 04NT02. http://dx.doi.org/10.1088/1361-6560/aafef0.

Elter, A., Dorsch, S., Thomas, S., Hentschke, C.M., Floca, R.O., Runz, A., Karger, C.P., Mann, P., 2021a. PAGAT gel dosimetry for everyone: Gel production, measurement and evaluation. Biomed. Phys. Eng. Express 7, 057001. http://dx.doi.org/10.1088/2057-1976/ac12a5.

Elter, A., Rippke, C., Johnen, W., Mann, P., Hellwich, E., Schwahofer, A., Dorsch, S., Buchele, C., Klüter, S., Karger, C.P., 2021b. End-to-end test for fractionated online adaptive MR-guided radiotherapy using a deformable anthropomorphic pelvis phantom. Phys. Med. Biol. 66, 245021. http://dx.doi.org/10.1088/1361-6560/ac3e0c.

Fong, P.M., Keil, D.C., Does, M.D., Gore, J.C., 2001. Polymer gels for magnetic resonance imaging of radiation dose distributions at normal room atmosphere. Phys. Med. Biol. 46, 3105–3113. http://dx.doi.org/10.1088/0031-9155/46/12/303.

GUM, 2008. Evaluation of measurement data—Guide to the expression of uncertainty in measurement (GUM). Joint committee for guides in metrology (JCGM). URL: https://www.bipm.org/documents/20126/2071204/JCGM_100_2008_E.pdf/cb0ef43f-baa5-11cf-3f85-4dcd86f77bd6.

Gustavsson, H., Bäck, S.J., Medin, J., Grusell, E., Olsson, L.E., 2004. Linear energy transfer dependence of a normoxic polymer gel dosimeter investigated using proton beam absorbed dose measurements. Phys. Med. Biol. 49, 3847–3855. http://dx.doi.org/10.1088/0031-9155/49/17/002.

Hayashi, K., Toyohara, M., Kusano, Y., Minohara, S., Shimono, Y., Gotoh, H., 2021. Behaviour and mechanism of micelle gel dosimeter for carbon-ion-beam irradiation. Radiat. Phys. Chem. 179, 109191. http://dx.doi.org/10.1016/j.radphyschem.2020.109191.

Hillbrand, M., Landry, G., Ebert, S., Dedes, G., Pappas, E., Kalaitzakis, G., Kurz, C., Würl, M., Englbrecht, F., Dietrich, O., Makris, D., Pappas, E., Parodi, K., 2019. Gel dosimetry for three dimensional proton range measurements in anthropomorphic geometries. Z. Med. Phys. 29, 162–172. http://dx.doi.org/10.1016/j.zemedi.2018.08.002.

Høye, E.M., Sadel, M., Kaplan, L., Skyt, P.S., Muren, L.P., Petersen, J.B.B., Swakoń, J., Mierzwińska, G., Rydygier, M., Malinowski, L., Balling, P., 2017. First 3D measurements of proton beams in a deformable silicone-based dosimeter. J. Phys. Conf. Ser. 847, 012021. http://dx.doi.org/10.1088/1742-6596/847/1/012021.

IAEA, 2000. Absorbed Dose Determination in External Beam Radiotherapy. Technical Reports Series 398, International Atomic Energy Agency, Vienna, Austria, p. 229.

Jäkel, O., 2020. Physical advantages of particles: Protons and light ions. Br. J. Radiol. 93, 20190428. http://dx.doi.org/10.1259/bjr.20190428.

Jaszczak, M., Kolesińska, B., Wach, R., Maras, P., Dudek, M., Kozicki, M., 2019. Examination of THPC as an oxygen scavenger impacting VIC dosimeter thermal stability and comparison of NVP-containing polymer gel dosimeters. Phys. Med. Biol. 64, 035019. http://dx.doi.org/10.1088/1361-6560/aafa86.

Kantemiris, I., Petrokokkinos, L., Angelopoulos, A., Bassler, N., Seimenis, I., Karaiskos, P., 2009. Carbon beam dosimetry using VIP polymer gel and MRI. J. Phys. Conf. Ser. 164, 012055. http://dx.doi.org/10.1088/1742-6596/164/1/012055.

Karger, C.P., Elter, A., Dorsch, S., Mann, P., Pappas, E., Oldham, M., 2024. Validation of complex radiotherapy techniques using polymer gel dosimetry. Phys. Med. Biol. 69, 06TR01. http://dx.doi.org/10.1088/1361-6560/ad278f.

Macchione, M.A., Lechón Páez, S., Strumia, M.C., Valente, M., Mattea, F., 2022. Chemical overview of gel dosimetry systems: A comprehensive review. Gels 8, 663. http://dx.doi.org/10.3390/gels8100663.

Maeyama, T., Fukunishi, N., Ishikawa, K.L., Fukasaku, K., Fukuda, S., 2016. Radiological properties of nanocomposite Fricke gel dosimeters for heavy ion beams. J. Radiat. Res. 57, 318–324. http://dx.doi.org/10.1093/jrr/rrw025.

Maeyama, T., Fukunishi, N., Ishikawa, K.L., Fukasaku, K., Fukuda, S., 2017. Organic-gelatin-free nanocomposite fricke gel dosimeter. J. Phys. Chem. B 121, 4238–4246. http://dx.doi.org/10.1021/acs.jpcb.6b11936.

Maeyama, T., Fukunishi, N., Ishikawa, K., Furuta, T., Fukasaku, K., Takagi, S., Noda, S., Himeno, R., Fukuda, S., 2014. A diffusion-free and linear-energy-transfer-independent nanocomposite Fricke gel dosimeter. Radiat. Phys. Chem. 96, 92–96. http://dx.doi.org/10.1016/j.radphyschem.2013.09.004.

Maeyama, T., Fukunishi, N., Ishikawa, K.L., Furuta, T., Fukasaku, K., Takagi, S., Noda, S., Himeno, R., Fukuda, S., 2015. Radiological characteristics of MRI-based VIP polymer gel under carbon beam irradiation. Radiat. Phys. Chem. 107, 7–11. http://dx.doi.org/10.1016/j.radphyschem.2014.09.001.

Maeyama, T., Hasegawa, H., Tanaka, M., Fukunishi, N., Ishikawa, K.L., Watanabe, Y., Fukuda, S., 2024. Linear-energy-transfer-independent nanoclay radio-fluorogenic gel dosimeter under energetic ion beams of $^{28}Si^{14+}$, $^{40}Ar^{18+}$, $^{56}Fe^{26+}$, $^{132}Xe^{54+}$, and $^{12}c^{6+}$. Radiat. Phys. Chem. 216, 111363. http://dx.doi.org/10.1016/j.radphyschem.2023.111363.

Maeyama, T., Mochizuki, A., Yoshida, K., Fukunishi, N., Ishikawa, K.L., Fukuda, S., 2023. Radio-fluorogenic nanoclay gel dosimeters with reduced linear energy transfer dependence for carbon-ion beam radiotherapy. Med. Phys. 50, 1073–1085. http://dx.doi.org/10.1002/mp.16092.

Mizukami, S., Watanabe, Y., Mizoguchi, T., Gomi, T., Hara, H., Takei, H., Fukunishi, N., Ishikawa, K.L., Fukuda, S., Maeyama, T., 2021. Whole three-dimensional dosimetry of carbon ion beams with an MRI-based nanocomposite fricke gel dosimeter using rapid T1 mapping method. Gels 7, 233. http://dx.doi.org/10.3390/gels7040233.

Ramm, U., Weber, U., Bock, M., Krämer, M., Bankamp, A., Damrau, M., Thilmann, C., Böttcher, H.D., Schad, L.R., Kraft, G., 2000. Three-dimensional BANG™ gel dosimetry in conformal carbon ion radiotherapy. Phys. Med. Biol. 45, N95–N102. http://dx.doi.org/10.1088/0031-9155/45/9/401.

Rousseau, A., Stien, C., Gouriou, J., Bordy, J.-M., Boissonnat, G., Chabert, I., Dufreneix, S., Blideanu, V., 2023. End-to-end quality assurance for stereotactic radiotherapy with Fricke-Xylenol orange-Gelatin gel dosimeter and dual-wavelength cone-beam optical CT readout. Phys. Medica 113, 102656. http://dx.doi.org/10.1016/j.ejmp.2023.102656.

Runz, A., Eboue Teto, R., Dinkel, F., Johnen, W., Elter, A., Dorsch, S., Echner, G., Karger, C.P., 2023. PO-1760 a low budget synthesis apparatus for reproducible production of dosimetry gels. Radiother. Oncol. 182, S1478–S1479. http://dx.doi.org/10.1016/S0167-8140(23)66675-7.

Simeonov, Y., Weber, U., Schuy, C., Engenhart-Cabillic, R., Penchev, P., Durante, M., Zink, K., 2021. Monte Carlo simulations and dose measurements of 2D range-modulators for scanned particle therapy. Z. Med. Phys. 31, 203–214. http://dx.doi.org/10.1016/j.zemedi.2020.06.008.

Stiefel, S., Heufelder, J., Pfaender, M., Lüdemann, L., Grebe, G., Heese, J., 2004. BANG®-polymergeldosimetrie in der protonentherapie von augentumoren. Z. Med. Phys. 14, 48–54. http://dx.doi.org/10.1078/0939-3889-00189.

Vedelago, J., Chacón, D., Romero, M., Venencia, D., Mattea, F., Valente, M., 2021. Dose-response of Fricke- and PAGAT-dosimetry gels in kilovoltage and megavoltage photon beams: Impact of LET on sensitivity. Phys. Medica 84, 41–49. http://dx.doi.org/10.1016/j.ejmp.2021.03.002.

Vedelago, J., Karger, C.P., Jäkel, O., 2022. A review on reference dosimetry in radiation therapy with proton and light ion beams: Status and impact of new developments. Radiat. Meas. 157, 106844. http://dx.doi.org/10.1016/j.radmeas.2022.106844.

Voit, D., Kalentev, O., Van Zalk, M., Joseph, A.A., Frahm, J., 2020. Rapid and motion-robust volume coverage using cross-sectional real-time MRI. Magn. Reson. Med. 83, 1652–1658. http://dx.doi.org/10.1002/mrm.28029.

Wang, X., Roeloffs, V., Merboldt, K.D., Voit, D., Schätz, S., Frahm, J., 2015. Single-shot multi-slice T1 mapping at high spatial resolution – inversion-recovery FLASH with radial undersampling and iterative reconstruction. Open Med. Imaging J. 9, 1–8. http://dx.doi.org/10.2174/1874347101509010001.

Weber, U., Kraft, G., 1999. Design and construction of a ripple filter for a smoothed depth dose distribution in conformal particle therapy. Phys. Med. Biol. 44, 2765–2775. http://dx.doi.org/10.1088/0031-9155/44/11/306.

Yao, C.-H., Huang, E.-Y., Juan, K.-J., Juang, P.-J., Juan, Y.-H., Chang, Y.-J., 2023. Feasibility evaluation of N-isopropyl acrylamide 3D gel dosimeters for proton therapy. PLoS One 18, e0291507. http://dx.doi.org/10.1371/journal.pone.0291507.

Zeidan, O.A., Sriprisan, S.I., Lopatiuk-Tirpak, O., Kupelian, P.A., Meeks, S.L., Hsi, W.C., Li, Z., Palta, J.R., Maryanski, M.J., 2010. Dosimetric evaluation of a novel polymer gel dosimeter for proton therapy. Med. Phys. 37, 2145–2152. http://dx.doi.org/10.1118/1.3388869.